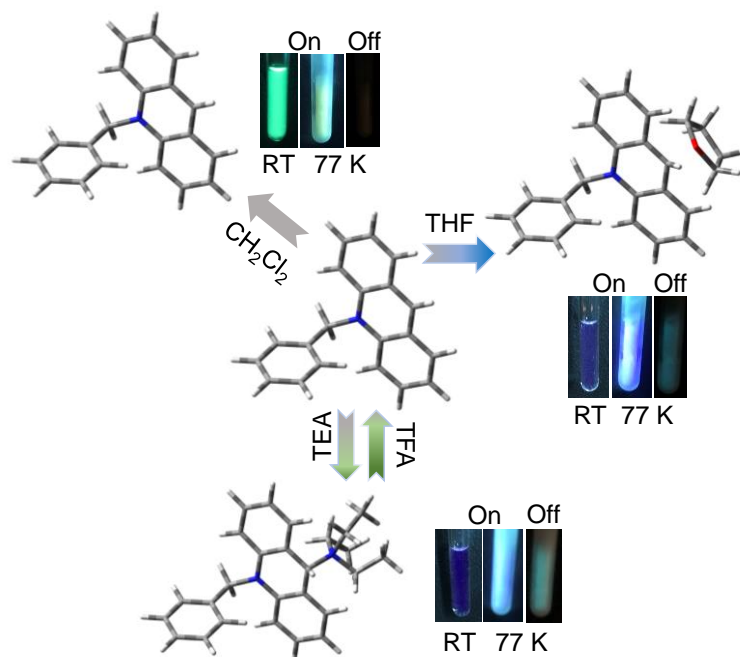


Phosphorescence Enables Identification of Electronic State for Acridinium Salt in Solutions

*Xiaolong Zhang, # Jiajun Du, # Fan Liao, Hao Su, Xuepeng Zhang, * and Guoqing Zhang**

ABSTRACT. Understanding intermolecular interactions between Lewis acid and base pairs is of fundamental importance in predicting non-covalent bonding and chemical reactivity. Here we show that an acridinium derivative, a Lewis acid, exhibits various degrees of interactions with Lewis bases of increasing nucleophilicity, including water (HOH), methanol (CH₃OH), tetrahydrofuran (ROR), amines (R₃N) and t-butoxide (RO⁻). Each interaction appears to result in a different type of solution state: solvation (e.g., water), coordination (e.g., tetrahydrofuran), chemical bonding (e.g., triethylamine), and radicals (e.g., t-butoxide). The solvated and coordinated acridinium molecules exhibit almost identical ¹H-NMR spectra, but possess drastically different UV absorption and luminescence emission, particularly phosphorescence; on the other hand, coordinated and chemically bonded acridinium species which are differentiated by heat calorimetry titration, share the same luminescence spectra but show two different sets of ¹H-NMR peaks. These distinct solution states could only be revealed by a combination of NMR and molecular fluorescence/phosphorescence spectroscopic methods, which could provide important clues in the mechanistic understanding of many important processes such as photo-redox reactions. The current report serves as an example of using phosphorescence spectroscopy as a complementary tool for characterizing electronic structures for interaction between organic molecules.

TOC GRAPHICS



Representation for molecular structures and Photoluminescence of ADBr and its interaction with dichloromethane, tetrahydrofuran, triethylamine.

KEYWORDS: Phosphorescence, Lewis acid, Lewis base, Bimolecular interaction, Acridinium

Acridinium salts (ADs) are an emerging class of organic photocatalysts, that are less expensive and more sustainable compared to their transition-metal complex counterparts, for a myriad of chemical reactions such as photooxidations, C-H functionalization, cross-coupling and cross-dehydrogenative reactions.¹ In 2004, Fukuzumi et al. pioneered in using ADs as an electron-transfer photocatalyst for efficient oxygenation reactions of anthracenes and olefins by taking advantage of the long-lived charge-separated state of the AD catalysts upon photoexcitation.² More recently, Nicewicz and co-workers developed ADs as a general photocatalyst for catalytic alkene anti-Markovnikov hydrofunctionalization

reactions.³ In addition, they have also achieved site-selective arene C-H amination and arene C-H fluorination via ADs-based photoredox catalysis, which could be of vital significance for pharmaceutical synthesis.⁴⁻⁸ In addition to the role as a photocatalyst separately, ADs have also been shown to work synergistically with other reagents in a dual-catalyst manner to activate “traditionally tough” reactions.⁹⁻¹¹ For instance, Wu et al. have utilized ADs in combination with a cobalt catalyst to engineer the Heck-type coupling between unactivated aliphatic acids and terminal alkenes.⁹ Rueping et al. have also integrated ADs with nickel catalysts for remote, site-specific arylation of ketones from easily accessible tertiary alcohols through C-C bond-cleaving cross-coupling.¹¹

One of the most predominant environmental parameters for catalysts performance is the solvation, *i.e.*, a change in solvent usually leads to altered reaction efficiency or main product, which is also true for AD catalysts. As stated by Alexanian et al., the C-H azidation in presence of ADs in 1,2-dichloroethane, 2,2,2-trifluoroethanol and hexafluoroisopropanol gave azidocyclooctane with yields of 30%, 50% and 70%, respectively, while maintaining the same condition for everything else.⁸ Similarly, Wu et al. described that the cross-coupling reaction between 3,3-dimethylbutanoic acid and styrene showed a high yield of >80% in toluene; however, low and mediocre yields of 12% and 61% were achieved in acetonitrile and (trifluoromethyl)benzene respectively.⁹ Nonetheless, most published reports focus mainly on screening the scope of substrates-products with respect to catalyst structures in reaction methodologies, with a lesser emphasis on the in-depth investigation on the role of solvent. One of the reasons for the lack of enthusiasm is perhaps due to the complexity in solvent-assisted organic reactions in general, and the fact that there are only

limited choices for solvents. As a result, the majority of proposed mechanisms to date were based on first-principles calculations.¹²

The special property about ADs is that they are extremely Lewis acidic due to a combination of an extended π -conjugation, and the presence of a positive charge, which lowers the π^* orbital. We thus expect that a small change in the electronic potential energy in the solvent could lead to a significant change in their interaction with ADs. Previously, we have shown that such Lewis acid-base pairing, revealed by single-crystal X-ray diffraction, could cause substantial changes in both ¹H-NMR and luminescence.¹³ Herein, by applying the same method, we reason that a combination of NMR and luminescence can also be used to reveal the electronic states of AD photocatalysts in the solution state. Using an acridinium bromide derivative (**ADBr**) as the core structure, we found that with increased nucleophilicity of the Lewis base, **ADBr** could in fact exhibit four drastically different electronic states, *i.e.*, solvation, coordination, chemical bonding and radical pair (Figure 1, **ADBr**). Compared to fluorescence spectroscopy, the phosphorescence spectrometry demonstrated its advantage in exploiting slow decay dynamics of the triplet excited state and cutting off interfering sources commonly seen for steady-state measurements.¹⁴⁻¹⁷ The multiple electronic states of ADs-Lewis base interactions revealed by abovementioned methods would have great implications in understanding a wide variety of reaction mechanisms concerning ADs photocatalysts.

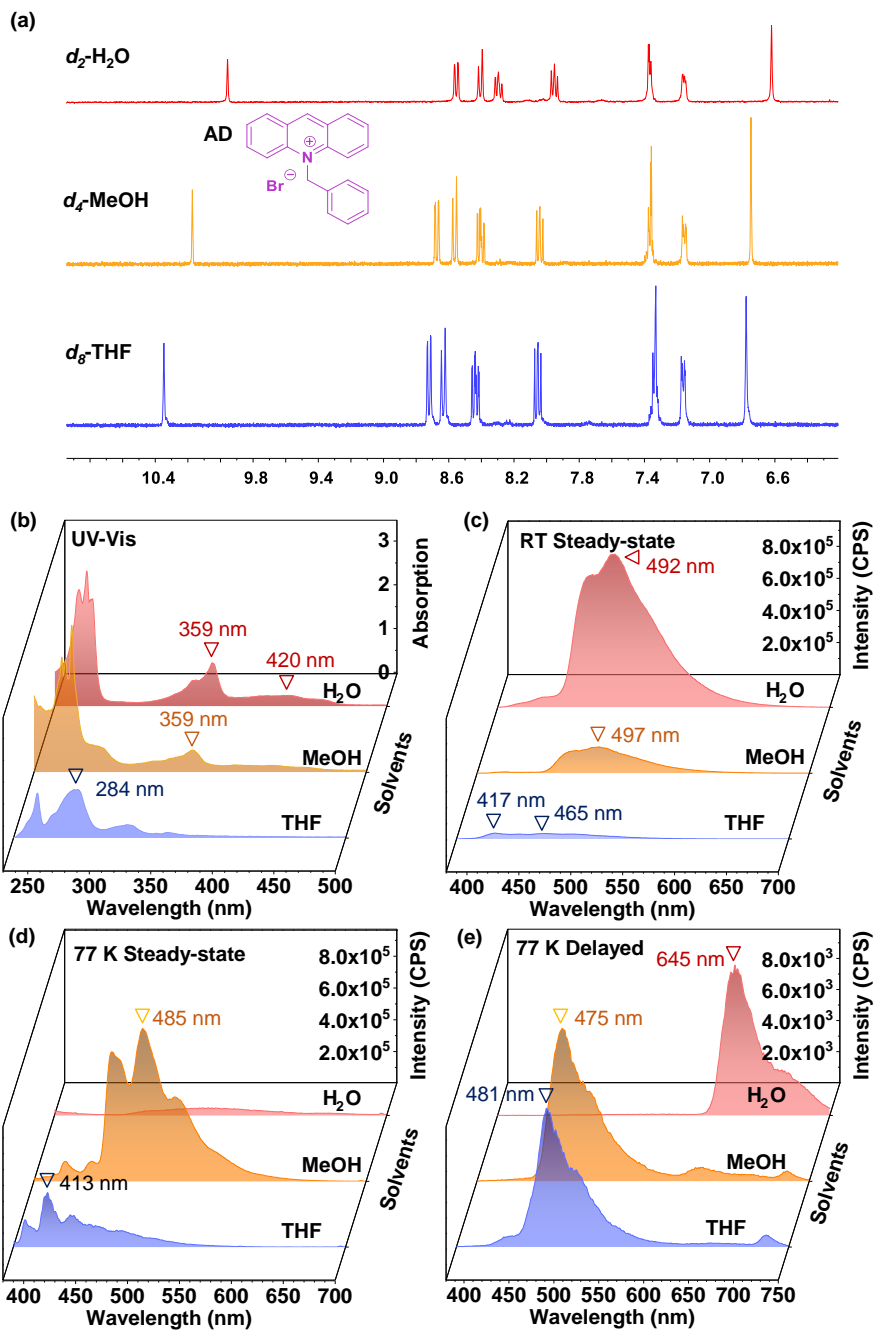


Figure 1. (a) ¹H NMR spectra of **ADBr** in d₂-H₂O, d₄-methanol and d₈-THF/d₆-DMSO (v/v = 6:1), respectively. (b) UV-vis absorption spectra of **ADBr** in water, methanol and THF, respectively. (c) Steady-state photoluminescence spectra of **ADBr** at room temperature in water, methanol and THF, respectively. Steady-state (d) and delayed (e)

photoluminescence spectra of **ADBr** at 77 K in water, methanol and THF, respectively ($\lambda_{\text{ex}} = 365 \text{ nm}$).

As shown in Figure 1a, the $^1\text{H-NMR}$ spectra of **ADBr** in three different deuterated solvents $\text{H}_2\text{O-d}_2$, MeOH-d_4 and THF-d_8 (for THF-d_8 , a mixed solvent with 86% DMSO-d_6 was used due to a limited solubility of **AD** in THF-d_8 alone) are almost identical except for minor shifts from proton peaks on the **AD** ring. Specifically, when the solvent becomes more Lewis basic (more electron-donating from $-\text{CD}_3$ or $-\text{CD}_2$), the proton signals from the **AD** ring moves downfield while those from the benzyl ring remain unchanged. It is noted that the peak of the hydrogen atom on the acridinium ring *para* to the N atom appears unusually sensitive to the solvent change (from 9.96 ppm in D_2O to 10.94 THF- d_8). The more dramatic de-shielding is very likely a consequence of stronger hydrogen bonding between the THF- d_8 oxygen lone pair and the aromatic proton *para* to the nitrogen, i.e., $\text{H}\dots\text{O}$, which decreases the $\text{H}\dots\text{O}$ distance and depletes the electron density around the hydrogen atom, which stems the Pauli exclusion principle.¹⁸ Despite the minor differences observed for the $^1\text{H-NMR}$ spectra, the corresponding UV-Vis spectra in the three non-deuterated solvents (Figure 1b), particularly between H_2O and THF, exhibit drastically differing patterns: in water, the lowest energy absorption extends to the visible region with well-defined vibronic structures (rendering the solution yellow to the naked eyes), attributed to the localized $\pi\text{-}\pi^*$ state of the acridinium ring. When the more electron-donating MeOH is used, the peak around $\sim 415 \text{ nm}$ is slightly weakened with a smeared vibronic feature, while a new shoulder band at $\sim 285 \text{ nm}$ emerges. For THF, however, the **ADBr** molecule seems to possess an almost completely different electronic configuration

in the ground state, as the absorption at 415 nm is largely displaced by a new set of peaks in the shorter wavelength region, indicating reduced π -conjugation size.

The two spectroscopic techniques on **ADBr** have so far resulted in apparently contradicting conclusions: $^1\text{H-NMR}$ data indicate little structural change (except for a slight variation in H bonding), but the UV-Vis data suggest, on the other hand, much reduced π -conjugation or some version of de-aromatization. The intriguing phenomenon prompted us to examine their fluorescence and phosphorescence spectra in these three solvents at both room and cryogenic temperatures (Figure 1c and 1d). The steady-state fluorescence spectrum at room temperature provides only limited information in that **ADBr** emission is gradually quenched in progressively more Lewis basic solutions, which could be due to photo-induced electron transfer (PET). Despite reduced emission intensity, the measured fluorescence lifetime, however, first exhibits a dramatic increase from 5.8 ns in water to 23.8 ns in methanol, and then decreases to 13.7 ns in THF, monitored at each emission maximum. The results indicate that the electronic transition becomes progressively more forbidden as the solvent becomes more nucleophilic. In combination with the UV-Vis spectra which suggest reduced electronic conjugation size, it could be inferred that the AD^+ ring may adopt a “diphenyl amine (DPA)” like structure rather than the planar AD^+ structure. At 77 K, however, **ADBr** in water is barely fluorescent ($\lambda_{\text{F}} = 530$ nm and $\tau_{\text{F}} = 8.5$ ns) but it shows strong steady-state emission in MeOH, where the fluorescence maximum is centred at 485 nm ($\tau_{\text{F}} = 27.5$ ns) with a minor peak around 411 nm. Conversely, the steady-state emission of **ADBr** in THF exhibits a dramatic hypsochromic shift to the deep blue region, with the emission maximum at 413 nm ($\tau_{\text{F}} = 1.5$ ns) and the peak around 485 nm ($\tau_{\text{F}} = 18.0$ ns) as the shoulder.

Up to this point, the hypothesis of nucleophilicity-induced de-aromatization still appears speculative based on a combination of NMR, UV-Vis and fluorescence spectra, given the possibility of reverse solvatochromic effect for charged organic molecules. The final piece of evidence arises from phosphorescence spectra, which were collected at a delay time of 1 ms (Figure 1e). The deep-red emission peaked at 645 nm with a shoulder around 700 nm is attributed to the triplet excited-state decay of the AD ring (with a calculated singlet-triplet energy gap, $\Delta E_{ST} = 0.42$ eV), which is consistent with previously published data and indicates unperturbed aromaticity in H₂O.¹⁹ For **ADBr** in MeOH, while NMR, UV-Vis and steady-state fluorescence spectra also suggest very little structural or electronic state change compared to **ADBr** in water, the main phosphorescence emission with an emission maximum around 475 nm reveals that a significant portion of **ADBr** molecules are in a different electronic state, which also dominates the **ADBr** phosphorescence emission in THF ($\lambda_P = 481$ nm, Figure 1e) at 77 K. Since both the emitting energy and vibronic spacing (1277 cm⁻¹) in the fluorescence and phosphorescence spectra of **ADBr** in THF at 77 K bear good resemblance of DPA.²⁰ If increased solvent nucleophilicity did induce DPA-like electronic structure for **ADBr**, one important question to ask is, whether THF forms a Lewis acid-base adduct (AD⁺...OR₂) or covalent bond (AD-OR⁺₂) with **ADBr**?

To answer this question, we selected a series of aromatic and aliphatic amines with different pK_a values (Figure S1), three representative ones of which are shown in Figure 2 (PhNH₂, DBU and TEA with an ascending order of nucleophilicity), to examine whether stronger Lewis bases (compared to THF) could chemically react with **ADBr**. It has to be noted that the experiment using amine controls cannot possibly produce an identical condition compared with the previous solvent one to allow for accurate NMR

measurements. Instead, an excess amount of amine (20 eq) was added to a CH₂Cl₂ solution (non-coordinating solvent) of **ADBr**. After addition of a weakly basic amine such as aniline, both the UV-Vis absorption and luminescence spectra show little change compared to those of **ADBr** alone in CH₂Cl₂; however, this does not necessarily indicate weaker nucleophilicity of aniline vs. THF toward **ADBr**, since we did not take into consideration of the concentration effect. Conversely, addition of amine with higher *pK_a* values such as DBU (11.5 in H₂O) and TEA (10.8 in H₂O), led to similar changes in UV-Vis absorption and luminescence spectra to those found for **ADBr** in THF (Figure 2a-2d). Specifically, the main UV-Vis absorption band shows a significant blue shift (284 nm) from the original 360 nm transition band. Meanwhile, the shoulder band extending well beyond 450 nm by **ADBr** in CH₂Cl₂ vanishes and is replaced by a new shoulder peak residing in between 300-350 nm, indicating smaller π conjugation forms after the addition of DBU or TEA at 20 eq. In contrast to the **ADBr** absorption in THF which still exhibits a small remnant peak \sim 360 nm, DBU and TEA presence eliminates such an absorption band as a result of much stronger association between an aliphatic amine and **ADBr**.

The room-temperature (RT) photoluminescence spectrum of **ADBr** with either DBU or TEA shows significantly decreased intensity, which again may be due to the PET effect (dynamic and/or static). The steady-state emission spectra of **ADBr**/DBU and **ADBr**/TEA in CH₂Cl₂ at 77 K possess vibronic progressions at 411 nm, 436 nm and 465 nm with the maximum peak at 411 nm. Consistently, the phosphorescence spectra of **ADBr**/DBU and **ADBr**/TEA in CH₂Cl₂ at 77 K present similar vibronic progressions to those of fluorescence and exhibit conspicuous blue shifts compared to that of **ADBr** alone in CH₂Cl₂.

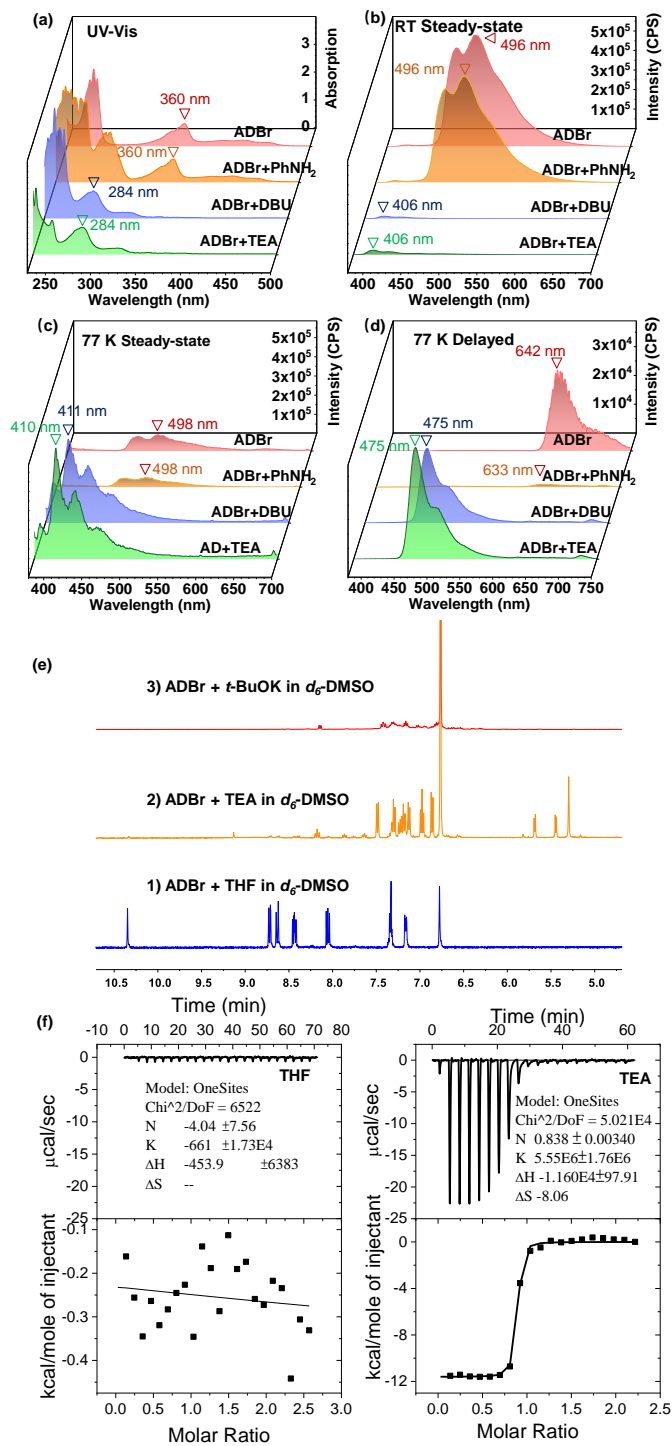


Figure 2. (a) UV-vis absorption spectra of **ADBr** in CH₂Cl₂ and that after addition of excess (1:20) of phenylamine, DBU and TEA, respectively. (b) Steady-state photoluminescence spectra of **ADBr** at room temperature in CH₂Cl₂ and that after adding of excess of

phenylamine, DBU and TEA, respectively. Steady-state (c) and delayed (d) photoluminescence spectra of **ADBr** at 77 K in CH₂Cl₂ and that after adding excess of phenylamine, DBU and TEA, respectively. (e) Isothermal titration calorimetry data of **ADBr** after addition of THF (left) and TEA (right), respectively, at 298 K.

As shown in Figure S1, the change in RT and 77 K photoluminescence spectra of **ADBr** after addition of n-butylamine, dibutylamine and piperidine are almost identical to that of **ADBr**/TEA in CH₂Cl₂, showing main emission peaks in the blue-shift region with DPA-like spectroscopic features. Conversely, the spectral change after addition of N, N-dibutylaniline was similar to that after addition of aniline, which resembles that of **ADBr** alone in CH₂Cl₂. To exclude possible deprotonation reaction between **ADBr** and a base, as shown in Figure 2e, the ¹H-NMR spectra of **ADBr** in d₆-DMSO with three different Lewis bases (THF, TEA and t-BuOK, respectively) were compared. Upon TEA addition (4 eq.), on the one hand, the **ADBr** benzyl group deprotonation was not observed, since a loss of the methylene proton results in an ylide with diminished NMR signal due to its diradical nature, as has been previously reported using a much stronger base, e.g., t-BuOK.²¹ On the other hand, the NMR spectrum of **ADBr**/TEA also varies substantially from that of **ADBr**/THF, where the signal of the proton para to the N atom at $\delta = 10.3$ ppm disappears, along with an ensemble high-field shift of aromatic protons from $\delta > 8$ ppm to 6.9-7.5 ppm (Figure 2e). The NMR results point to a highly likely event of chemical reaction between TEA and **ADBr**.

To further verify the nature of interactions between **ADBr** with THF and TEA, respectively, an isothermal titration calorimetry analysis was carried out for both systems of **ADBr** /THF and

ADBr/TEA in CH₂Cl₂. During the monitored course of 80 min, the CH₂Cl₂ solution containing THF and **ADBr** (Figure 2f) shows negligible enthalpy change, indicating no sign of chemical reactions. In contrast, the **ADBr**/TEA combination in CH₂Cl₂ lead to an enthalpic change that is larger than that of **ADBr**/THF combination in CH₂Cl₂ by two orders of magnitude. The measured enthalpic change $\Delta H = -11.6$ kcal/mol with an entropic change of $\Delta S = -8$ cal/mol is consistent with a spontaneous (calculated $\Delta G = -9.3$ kcal/mol) nucleophilic addition reaction between TEA and **ADBr** at a 1:1 ratio (Figure 2f). It has to be noted that there is a trace amount of impurities, the NMR spectrum of which were compared with that of acridone (Figure S2) in the aromatic region giving a positive match. This could provide a clue to the whereabouts of the TEA addition site, *i.e.*, the carbon para to the acridinium nitrogen, given that acridone has been known to form following nucleophile addition and subsequent oxidization in the presence of water and oxygen.¹⁸

To substantiate the hypothesis of TEA addition induced acridone formation, ¹H-NMR and UV-vis spectra were employed. As shown in Figure 3a, the ¹H-NMR spectrum of **ADBr**/TEA in d₆-DMSO after 10 min could be restored to the initial state, by way of neutralization from a strong acid such as trifluoroacetic acid (TFA) or hydrochloric acid (HCl). However, the acridone impurity was stable with TEA, which was also verified with ¹H-NMR (Figure S3). Correspondingly, the UV-Vis absorption spectrum of **ADBr**/TEA also developed into a profile that is almost identical to **ADBr** alone in CH₂Cl₂ upon HCl titration, with an isosbestic point at 325 nm (Figure 3b). However, the two doublet peaks at 5.69 and 5.44 ppm in the NMR spectrum of **ADBr**/TEA also suggest two alternative possible nucleophilic addition sites as shown in Scheme 1, which then produce a set of protons attached to non-aromatic double bonds.

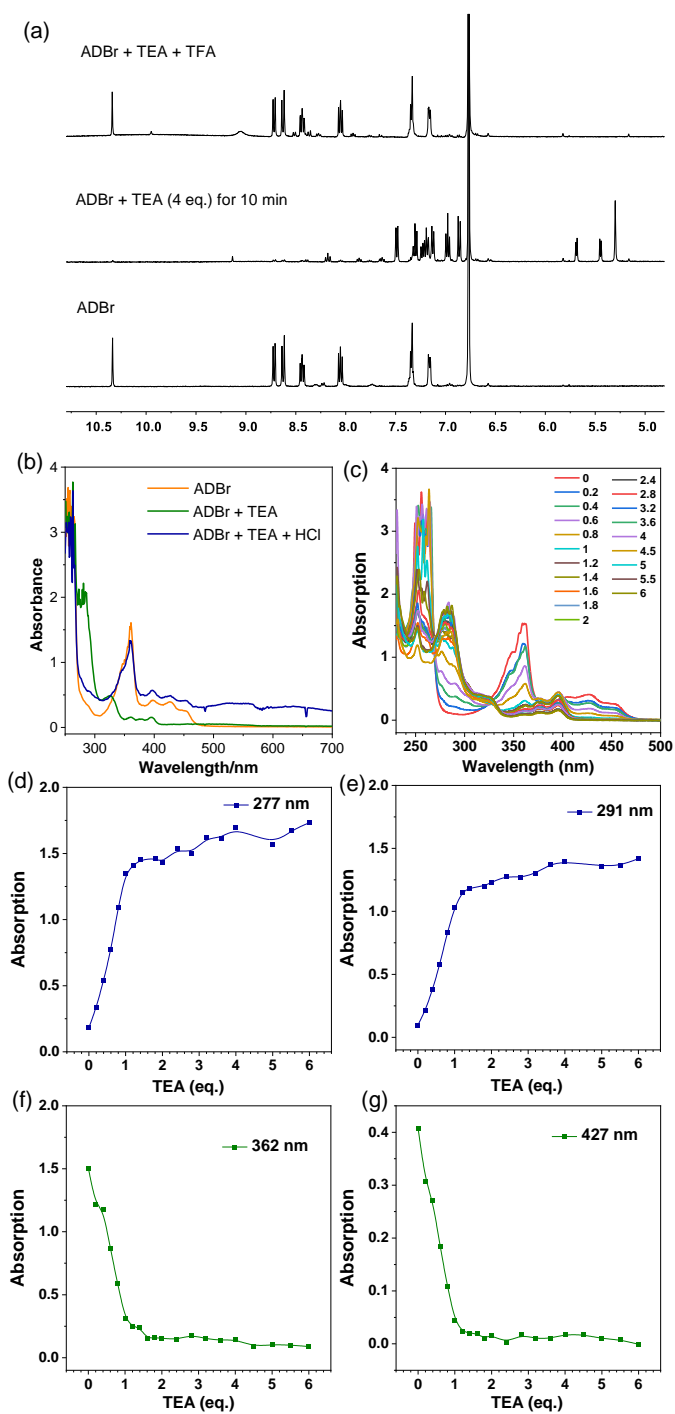
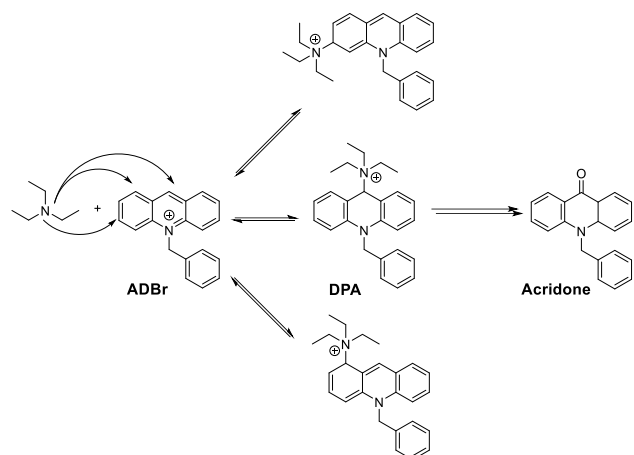


Figure 3. (a) ^1H NMR spectra of **ADBr** in $\text{d}_6\text{-DMSO}$ after addition of TEA and subsequent addition of TFA, respectively. (b) UV-vis absorption spectra of **ADBr** in CH_2Cl_2 after addition of TEA and subsequent addition of HCl, respectively. (c) UV-vis absorption spectra of **ADBr** in CH_2Cl_2 after

addition of different molar ratio of TEA. (d)~(g) Corresponding intensity changes of the absorption at 277 nm, 291 nm, 362 nm and 427 nm, respectively.



Scheme 1. Proposed addition and oxidation products when excess triethylamine (4 eq) was added into the **ADBr** solution in d_6 -DMSO.

In summary, four different types of interactions between an acridinium bromide salt and various Lewis bases were identified by a combination of NMR and fluorescence/phosphorescence spectroscopic characterization, including solvation, coordination, chemical bonding and radical pair. Most interestingly, the coordination state and bonding state exhibit almost identical electronic transitions but with very different nuclear organizations. The multiple electronic states of the AD core under different surroundings might provide important clues for understanding the role of solvents and aid the design for better ADs photocatalyst in the future. Attempting to understand more complicated Lewis acid-Lewis base interactions by such experimental techniques is underway.

ASSOCIATED CONTENT

Supporting Information.

The Supporting Information is available free of charge at <https://pubs.acs.org>

AUTHOR INFORMATION

Corresponding Authors

Xuepeng Zhang – Hefei National Laboratory for Physical Sciences at the Microscale, University of Science and Technology of China, Hefei 230026, China;

Email: zhangxp@ustc.edu.cn

Guoqing Zhang – Hefei National Laboratory for Physical Sciences at the Microscale, University of Science and Technology of China, Hefei 230026, China;

Email: gzhang@ustc.edu.cn

Notes

The authors declare no competing financial interests.

These authors contributed equally to this work.

ACKNOWLEDGMENT

This work is supported by the National Key R&D Program of China (2017YFA0303500), the National Natural Science Foundation of China (21975238 and 22003063) and the startup fund from University of Science and Technology of China (KY2340000139).

REFERENCES

- (1) Tlili, A.; Lakhdar, S. Acridinium Salts and Cyanoarenes as Powerful Photocatalysts: Opportunities in Organic Synthesis. *Angew. Chem. Int. Ed.* **2021**, 60, 19526-19549.
- (2) Kotani, H.; Ohkubo, K.; Fukuzumi, S. Photocatalytic Oxygenation of Anthracenes and Olefins with Dioxygen via Selective Radical Coupling Using 9-Mesityl-10-methylacridinium Ion as an Effective Electron-Transfer Photocatalyst. *J. Am. Chem. Soc.* **2004**, 126, 15999-16006.
- (3) Margrey, K. A.; Nicewicz, D. A. A General Approach to Catalytic Alkene Anti-Markovnikov Hydrofunctionalization Reactions via Acridinium Photoredox Catalysis. *Acc. Chem. Res.* **2016**, 49, 1997-2006.
- (4) Tay, N. E. S.; Chen, W.; Levens, A.; Pistritto, V. A.; Huang, Z.; Wu, Z.; Li, Z.; Nicewicz, D. A. ^{19}F - and ^{18}F -arene deoxyfluorination via organic photoredox-catalysed polarity-reversed nucleophilic aromatic substitution. *Nature Catalysis*, **2020**, 3, 734-742.
- (5) Wilger, D. J.; Grandjean, J. M. M.; Lammert, T. R.; Nicewicz D. A. The direct anti-Markovnikov addition of mineral acids to styrenes. *Nature Chemistry*, **2014**, 6, 720-726.
- (6) Romero, N. A.; Margrey, K. A.; Tay, N. E.; Nicewicz, D. A. Site-Selective Arene C-H Amination Via Photoredox Catalysis. *Science*, **2015**, 349, 1326-1330.
- (7) Chen, W.; Huang, Z.; Tay, N. E. S.; Giglio, B.; Wang, M.; Wang, H.; Wu, Z.; Nicewicz, D. A.; Li, Z. Direct arene C-H fluorination with ^{18}F -via organic photoredox catalysis. *Science*, **2019**, 364, 1170-1174.
- (8) Margrey, K. A.; Czaplyski, W. L.; Nicewicz, D. A.; Alexanian, E. J. A General Strategy for Aliphatic C-H Functionalization Enabled by Organic Photoredox Catalysis. *J. Am. Chem. Soc.* **2018**, 140, 4213-4217.

- (9) Cao, H.; Jiang, H.; Feng, H.; Kwan, J. M. C.; Liu, X.; Wu, J. Photo-induced Decarboxylative Heck-Type Coupling of Unactivated Aliphatic Acids and Terminal Alkenes in the Absence of Sacrificial Hydrogen Acceptors. *J. Am. Chem. Soc.* **2018**, 140, 16360-16367.
- (10) McManus, J. B.; Griffin, J. D.; White, A. R.; Nicewicz, D. A. Homobenzylic Oxygenation Enabled by Dual Organic Photoredox and Cobalt Catalysis. *J. Am. Chem. Soc.* **2020**, 142, 10325-10330.
- (11) Huang, L.; Ji, T.; R. M. Remote Nickel-Catalyzed Cross-Coupling Arylation via Proton-Coupled Electron Transfer-Enabled C-C Bond Cleavage. *J. Am. Chem. Soc.* **2020**, 142, 3532-3539.
- (12) Fukuzumi, S.; Kotani, H.; Ohkubo, K.; Ogo, S.; Tkachenko, N. V.; Lemmetyinen, H. Electron-Transfer State of 9-Mesityl-10-methylacridinium Ion with a Much Longer Lifetime and Higher Energy Than That of the Natural Photosynthetic Reaction Center. *J. Am. Chem. Soc.* **2004**, 126, 1600-1601.
- (13) Sun, X.; Zhang, B.; Li, X.; Trindle, C. O.; Zhang, G. External Heavy-Atom Effect via Orbital Interactions Revealed by Single-Crystal X-ray Diffraction. *J. Phys. Chem. A* **2016**, 120, 5791-5797.
- (14) Huang, W.; Zhang, X.; Chen, B.; Miao, H.; Trindle, C. O.; Wang, Y.; Luo, Y.; Zhang, G. Boosting the triplet activity of heavy-atom-free difluoroboron dibenzoylmethane via sp^3 oxygen-bridged electron donors. *Chem. Comm.* **2019**, 55 (1), 67-70.
- (15) Chen, B.; Zhang, X.; Wang, Y.; Miao, H.; Zhang, G. Aggregation-Induced Emission with Long-Lived Room-Temperature Phosphorescence from Methylene-Linked Organic Donor-Acceptor Structures, *Chem. Asian J.* **2019**, 14 (6), 751-754.

- (16) Zhang, X.; Xie, T.; Cui, M.; Yang, L.; Sun, X.; Jiang, J.; Zhang, G. General design strategy for aromatic ketone-based single-component dual-emissive materials. *ACS Appl. Mater. Interfaces* **2014**, 6 (4), 2279-2284.
- (17) Chen, X.; Xu, C.; Wang T.; Zhou, C.; Du, J.; Wang, Z.; Xu, H.; Xie. T.; Bi, G.; Jiang, J.; Zhang, X.; Demas, J. N.; Trindle, C. O.; Luo, Y.; Zhang, G. Versatile room temperature phosphorescent materials prepared from N-substituted naphthalimides: emission enhancement and chemical conjugation, *Angew. Chem. Int. Ed.* **2016**, 55 (34), 9872-9876.
- (18) Zarycz, M. N. C.; Guerra, C. F. NMR ¹H-Shielding Constants of Hydrogen-Bond Donor Reflect Manifestation of the Pauli Principle. *J. Phys. Chem. Lett.* 2018, 9, 3720-3724.
- (19) Benniston, A. C.; Harriman, A.; Li, P.; Rostron, J. P.; Ramesdonk, H. J.; Groeneveld, M. M.; Zhang, H.; Verhoeven, J. W. Charge Shift and Triplet State Formation in the 9-Mesityl-10-methylacridinium Cation. *J. Am. Chem. Soc.* **2005**, 127, 16054-16064.
- (20) Kasha, M. Transmission Filters for the Ultraviolet. *J. Opt. Soc. Am.*, **1948**, 38, 929-934.
- (21) Liao, F.; Huang, W.; Chen, B.; Ding, Z.; Li, X.; Su, H.; Wang ,T.; Wang, Y.; Miao, H.; Zhang, X.; Luo, Y.; Zhang, G. Are pyridinium ylides radicals? *Chem. Comm.* **2020**, 56 (76), 11287-11290.